SEVENTH FRAMEWORK PROGRAMME

CAPACITIES - ERA.Net RUS: Linking Russia to the ERA

Contract for: **Innovation Project**

D.5.2

EO Data Analysis Protocol (HR-LR)

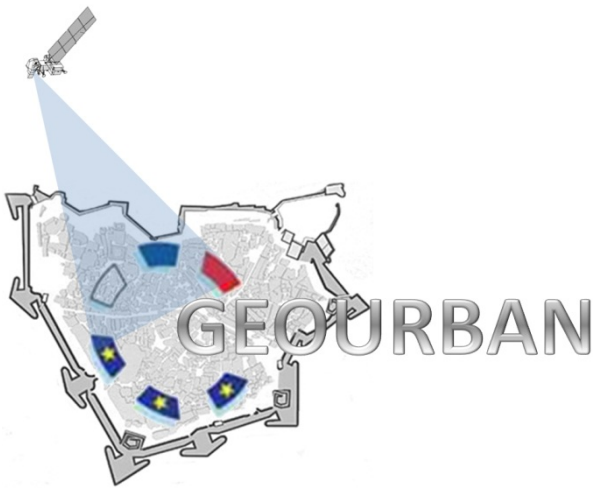

Project acronym: **GEOURBAN**
Project full title: Exploitin**G** **E**arth **O**bservation in s**U**stainable u**RB**an pl**A**nning & ma**N**agement
Contract no.: ERA.Net-RUS-033
Date: 28/02/2013

Doc.Ref.: GEOURBAN_05_DD_UNIBAS

Book Captain: Christian Feigenwinter

Contributors: Eberhard Parlow, Dimitrios Triantakonstantis, Nektarios Chrysoulakis

Issue: 1.1

Deliverable no.: D.5.2

Dissemination: PT

Document Status Sheet

Issue	Date	Author	Comments
1.0	20/02/2013	C. Feigenwinter	Draft out for consortium review
1.1	28/02/2013	C. Feigenwinter, E. Parlow, D. Triantakonstantis N. Chrysoulakis	Final version

Table of Contents

1. WORKPACKAGE OVERVIEW

WP5 includes the **local and regional applications** in GEOURBAN case studies. As in the case of VHR data, previous research projects already addressed the use of high spatial resolution (HR) EO data in local scale applications such as land cover mapping and change detection, as well as the use of low spatial resolution (LR) EO in regional scale applications such aerosol concentration estimation. WP5 represents a unique attempt to collect and to analyze an integrated EO dataset suitable for the evaluation of a subset of the EO-based indicators developed in WP3. As in WP4, the development of EO data analysis techniques is beyond the scope of GEOURBAN, therefore state of the art methods will be used to derive specific products from raw EO datasets. In case of regional scale where EO derived products are already available online (i.e. MODIS Level 2 products) these products will be directly used. The output of this WP is a set of products to be used as inputs for indicator evaluation and a report on both the techniques used to derive these products from raw EO data and the location of the online available EO-derived products (deliverable D.5.2).

WP5 also involves the description of the **Earth Observation Products Database** for GEOURBAN case studies. The ability to design associated applications is critical to the success of the database. Identification of requirements and specifications related to the use of EO products provides the users with a high-level understanding of the GEOURBAN products. Hence, WP5 together with WP4 provide a design of database for a better sharing of GEOURBAN outputs. A conceptual database design is presented which involves modeling the relations between the raw EO data, EO-based indicators and EO products obtained from processing of VHR, HR and LR resolution EO raw data (deliverable D.5.1).

1.1. Purpose of the document

This document is the deliverable D.5.2 **Earth Observation Data Analysis Protocol (HR-LR)** of the GEOURBAN Project. It provides the protocol for the use of high resolution (HR) and low resolution (LR) images to drive EO-based indicators to guide end-users. Information about the general characteristics of HR EO images and the algorithms used for information extraction is presented.

1.2. Definitions and acronyms

Acronyms

AATSR	Advanced Along Track Scanning Radiometer
AOT/AOD	Aerosol Optical Thickness/Aerosol Optical Depth
BRDF	Bidirectional Reflectance Distribution Function
DEM	Digital Elevation Model
DN	Digital Number
DSM	Digital Surface Model
EO	Earth Observation
FLAASH	Fast Line-of-sight Atmospheric Analysis of Spectral Hypercubes
LAADS	Atmosphere Archive and Distribution System
LSE	Land Surface Emissivity
LST	Land Surface Temperature
MERIS	Medium Resolution Imaging Spectrometer
MODIS	Moderate Resolution Imaging Spectrometer
MODTRAN	Moderate resolution atmospheric transmission
NASA	National Aeronautics and Space Administration
NDVI	Normalized Difference Vegetation Index
ROI	Region of Interest
SRTM	Shuttle Radar Topography Mission
TM/ETM+	Thematic Mapper/Enhanced Thematic Mapper
TOA	Top-Of-Atmosphere
UHI	Urban Heat Island
USGS	U.S. Geological Survey

1.3. Document references

GEOURBAN D.1.1 Project Management Plan, 30/03/2012

GEOURBAN D.2 Urban planning requirements 04/10/2012

GEOURBAN D.4.2 EO data analysis protocol (VHR) 30/11/2012

GEOURBAN D.5.1 EO products database (HR-LR) 28/12/2012

Abrams, M., B. Bailey, H. Tsu, and Hato, M., 2010. The ASTER Global DEM. *Photogrammetric Engineering and Remote Sensing*, 76, 344 - 348.

Artis, D.A., Carnahan, W.H., 1982. Survey of emissivity variability in thermography of urban areas. *Remote Sensing of Environment*, 12, 313-329

Campbell, J.B., 2002. Introduction to Remote Sensing. 3rd edition, Taylor and Francis, London.

Carlson, T.N., Ripley, D.A., 1997. On the relation between NDVI, fractional vegetation cover, and leaf area index. *Remote Sensing of Environment*, 62, 241-252

Chander, G., Markham, B.L., Helder, D.L., 2009. Summary of current radiometric calibration coefficients for Landsat MSS, TM, ETM+ and EO-1 ALI sensors. *Remote Sensing of Environment*, 113, 893-903

Chrysoulakis, N., Abrams, M., Kamarianakis, Y. and Stanisławski, M., 2011. Validation of the ASTER GDEM for the area of Greece. *Photogrammetric Engineering & Remote Sensing*, 77, 157 - 165.

Congalton, R.G., 1991. A review of assessing the accuracy of classifications of remotely sensed data. *Remote Sensing of Environment*, 37, 35-46

Farr, T. G., et al., 2007. The Shuttle Radar Topography Mission, *Reviews of Geophysics*, 45, DOI: 10.1029/2005RG000183

Forster, B., 1983. Some urban measurements from Landsat data. *Photogrammetric Engineering and Remote Sensing*, 49, 1693–1707.

Gillespie, A.R., Rokugawa, S., Hook, S., Matsunaga, T., Kahle, A.B. 1998. A temperature and emissivity separation algorithm for ASTER images. *IEEE Transactions on Geoscience and Remote Sensing,* 36, 1113-1126

Liang, S., 2000. Narrowband to broadband conversions of land surface albedo: I. Algorithms. *Remote Sensing of Environment*, 76, 213-238

Liang, S. et al., 2002. Narrowband to broadband conversions of land surface albdo: II. Validation. *Remote Sensing of Environment*, 84, 25-41

Prata, A.J., Caselles, V., Coll, C., Sobrino, J.A., Ottle, C., 1995. Thermal remote sensing of land surface temperatures from satellites : Current status and future prospects. *Remote Sensing Reviews*, 12, 175-224

Remer, L.A. and co-authors, 2005. The MODIS Aerosol Algorithm, Products, and Validation. *Journal of the Atmospheric Sciences-Special Section,* 62, 947-973

Richards, J.A., 1999. Remote Sensing Digital Image Analysis, Springer, Berlin, p. 240

Stehman, S.V., 1996. Estimating the Kappa coefficient and its variance under stratified random sampling. *Photogrammetric Engineering and Remote Sensing*, 62, 401–402.

Sobrino, J.A., Jiménez-Muñoz, J.C., Paolini, L., 2004. Land surface temperature retrieval from LANDSAT TM 5, *Remote Sensing of Environment*, 89, 467–483

Wan, Z., 2007. Collection-5 MODIS Land Surface Temperature Products User's Guide. http://www.icess.ucsb.edu/modis/LstUsrGuide/MODIS_LST_products_Users_guide_C5.pdf (last accessed FEB 27 2013)

Weng, Q., Lu, D. and Schubring, S., 2004. Estimation of land surface temperature-vegetation abundance relationship for urban heat island studies. *Remote Sensing of Environment*, 89, 467–483

NASA, 2011. Landsat Science Data Users Handbook. http://landsathandbook.gsfc.nasa.gov (last accessed FEB 27 2013)

FLAASH Module User's Guide, 2009. Atmospheric Correction Module: QUAC and FLAASH User's Guide, Version 4.7. ITT Visual Information Solutions Inc. http://www.exelisvis.com/portals/0/pdfs/envi/Flaash_Module.pdf (last accessed FEB 27 2013)

USGS EarthExplorer: http://earthexplorer.usgs.gov/

USGS Global Visualization Viewer (Glovis): http://glovis.usgs.gov/

2. DESCRIPTION OF HR-LR EO DATA AND PRODUCTS

The EO data and related products involve mainly the georeferenced EO satellite images and their processed outputs which are obtained by using various image processing algorithms which are described in section 3. The processed images of EO data form the basis of indicators to be used in the GEOURBAN framework. These products are obtained for the case studies Basel, Tyumen and Tel Aviv according to available EO data in various spatial resolutions. Table 1 indicates the available data and obtained products.

Available EO data	Spatial resolution		Spectral resolution or product	Processed products
Landsat TM (ETM+)	VIS B G R NIR SWIR Thermal Panchromatic (ETM+ only)	30 m 120 m (60 m) 15 m	0.485 μm 0.560 μm 0.660 μm 0.830 μm 1.650 μm 2.220 μm 11.450 μm 0.7199 μm	Land cover/Land use (LULC), land surface temperature and emissivity (LST/LSE), broadband albedo, NDVI
SRTM		90 m	DTM	DTM
GDEM		30 m	ASTER Global DEM	DTM
MODIS		250 m	36 spectral bands 0.405-14.385 μm	
		1000 m	MOD/MYD11 A2	LST day, LST night
		500 m	MCD12	Land cover
		10000 m	MOD/MYD04_L2 Aerosol product	Aerosol optical thickness AOT

Table 1. HR-LR EO data and products for GEOURBAN case studies

EO products are mainly land use/land cover (LULC) as well as surface features of urban areas (LST, albedo, NDVI), which are in the form of raster images. All the raster EO products are provided in Geotiff format with WGS84 datum and UTM coordinate system.

3. EO PRODUCTS AND ALGORITHMS

3.1. Landsat TM, ETM+

As the primary source of medium spatial resolution Earth observations used in decision-making the Landsat satellite series provide an invaluable inventory for monitoring the global land surface and its natural and human-induced landscape changes. The Landsat data archive at the U.S. Geological Survey (USGS) Earth Resources Observation and Science (EROS) Center holds an unequaled 40-year record of the Earth's surface and is freely available to users via the EarthExplorer or the Global Visualization Viewer (GloVis) web sites. The GEOURBAN project uses this extraordinary database.

Preprocessing of Landsat TM and ETM+ data was done using the current equations and rescaling factors for converting calibrated digital numbers (DNs) to absolute units of at-sensor spectral radiance, Top-Of-Atmosphere (TOA) reflectance, and at-sensor brightness temperature as described in Chander et al. (2009) and implemented in the ENVI software package. Scaling factors for TM and ETM+ are also available from the meta-information are delivered with Landsat scenes (MTL.txt files).

If surface reflectance is required as input for a product algorithm (e.g. broadband albedo), an atmospheric correction has to be applied to convert at-sensor radiance to surface spectral reflectance. Atmospheric correction was applied with the FLAASH (Fast Line-of-sight Atmospheric Analysis of Spectral Hypercubes) module implemented in ENVI software. FLAASH is based on MODTRAN4 code (FLAASH, 2009). Since most scenes were scanned under clear sky conditions, a mid-latitude summer atmosphere with a visibility of 60 km and rural aerosol model was applied for the Basel case study.

3.2. Landsat TM/ETM+ derived products

3.2.1 Land use/Land cover (LULC)

Land use/Land cover (LULC) is a key product in GEOURBAN. Several indicators (e.g. fractional land cover, land cover change, built-up density, etc.), as defined in deliverable D.3, rely on derivatives of LULC and thus their quality depends on the quality and

accuracy of the LULC classification. The numerous methods to perform a LULC analysis can be roughly divided in two main approaches: supervised and unsupervised. Whichever method is chosen for LULC classification, post classification algorithms have to be applied. Though LULC classification algorithms are well established in literature and a large number of methods is implemented in standard remote sensing and GIS software packages, “fine tuning” of the first results is inevitable and probably the most important step in all approaches, i.e. the applied method has to be adapted to the specific scene to be analyzed and to the specific needs of the user to receive the appropriate result at the end of the processing chain. For a comparison of common classifiers refer also to GEOURBAN deliverable D.4.2, section 3.

In the frame of GEOURBAN, we recommend the application of a supervised image classification, the Maximum Likelihood Classifier (MLC), but any other supervised classifier may be applied. MLC has been proven to deliver robust results. Supervised classification in general is essentially a three-step process:

First, a number of well-distributed, representative training pixels have to be located for each class in the scene under consideration. The pixels of these training areas, also known as “region of interest” (ROI), are used for the calculation of descriptive class statistics (e.g. average and variability). The choice of ROIs is crucial and has significant impact on the quality of the classification result. It must therefore be applied with care. The spectral separability between selected ROI pairs provides a measure of the discrimination of the two classes and can be computed for given input data. In ENVI both, the Jeffries-Matusita and the Transformed Divergence separability measures are reported (Richards, 1999). Output values range from 0 to 2.0 indicating how well the selected pairs are statistically separate. Values greater than 1.9 indicate good separability, for lower separability values a re-editing of ROIs is recommended and pairs with separability values lesser than one may be combined into a single class. Due to the spectral properties of urban surface materials, these thresholds have to be reconsidered, especially if a differentiation between several degrees of residential density is desired (e.g. classes 4-6 in table 2). The separability values between these classes are normally lower than one. Nevertheless, the obtained results suggest that such a detailed classification is accurate enough for certain applications. If the accuracy is not satisfying enough, the user may still combine classes 4-6 into one single residential class. Other low separability values are

reported for certain agricultural land use (e.g. vineyards) and the low residential class, mainly located in peri-urban regions.

In a second step each pixel is assigned to the class with the greatest similarity, as defined in the chosen classifier's decision rules. In MLC for example, a pixel is labeled as belonging to the class with the highest posterior probability of membership (e.g. Campbell, 2002). The user has the possibility to define different probability values for each class, if desired.

In a third step the accuracy of the classification is assessed with respect to a set of independent reference pixels. The end result of the classification is a thematic map with the distribution of the selected classes that usually comes together with an estimation of the accuracy. The quality of such a product depends on several factors related to the applied methods as well as to the nature of the selected classes and the quality of EO-data.

There are some points to keep in mind when performing LULC classification in general and of urban areas in part. Cleary, any conventional classifier (including MLC) assumes that the scene under consideration is a composition of unique and homogeneous classes that are mutually exclusive. However, in reality such assumptions are generally invalid and most land cover types are subject to significant fuzziness, especially in urban environments. Fuzziness also occurs due to the presence of mixed pixels which are not occupied by a single, homogenous category. The complex relationship between at-sensor spectral responses and the corresponding ground situations can cause additional problems: similar entities at different locations may exhibit different spectral responses, while similar spectral responses may relate to different entities (Forster, 1983). Thus, even if the classes are discrete and mutually exclusive on the ground, they may be mixed in the representation provided by the remotely sensed imagery. Though there may be more sophisticated supervised classifiers than MLC based on more complex techniques like e.g. neural networks or support vector machines, the quality of the final products is comparable due to our experience in GEOURBAN case studies. In fact, selecting appropriate training areas and an attentive post classification seem to be the most crucial steps that affect the quality of a classification.

Supervised classification algorithms are preferably applied on surface reflectance data in order to reduce the effect of different acquisition conditions. We therefore recommend

preprocessing of the input data as described in section 3.1 (calibration and atmospheric correction), although it is also possible to use the raw data as an input for MLC.

Step 1: In a first step ROIs are selected for the LULC classes listed in table 2 and a first MLC is performed. Note that several additional sub-classes (see fig. 1) have to be introduced especially for the agricultural land use class and possibly for forests in this step. As mentioned before, the most problematic classes are the three residential classes and the low density residential class in peri-urban regions which coincides with specific agricultural land use (e.g. wine yards). In fact, the spectral signature of these two classes is very similar and reflects the composition of surface materials common to both classes, namely green vegetation, bare soil, stone or other construction materials, and their relative contributions to the total spectral response of such a pixel.

As already mentioned the choice of endmembers is crucial. We recommend using the same areas for residential and industrial classes in the different scenes to be analyzed, if possible. This implies that a chosen ROI for e.g. a high density residential or an industrial area should correspond to the respective class in all scenes under investigation. It is therefore advisable to start with the oldest scene. Note that in any case, ROIs have to be checked thoroughly in each scene, if they still match the respective class. Step 1 may be repeated until the degree of misclassifications is minimized by visual inspection. Sub-classes are then integrated into one of the 10 classes in Table 2.

DN	combined	R	G	B	ENVI color table
0	unclassified				
1	forest I	0	139	0	green III
2	water body	0	0	255	blue
3	agriculture I	238	238	0	yellow I
4	residential I high density	238	0	0	red I
5	residential II	205	0	0	red II
6	residential III low density	139	0	0	red III
7	grassland	0	255	0	green
8	clouds	255	255	255	white
9	clouds shadow	85	26	139	purple III
10	industrial/commercial	255	165	0	orange I

Table 2: Land use/Land cover classes in GEOURBAN case studies.

Step 2: Different steps of post-processing can be applied once the result of MLC is satisfying. Post-processing includes techniques like sieving (eroding) and clumping (dilating) classes and/or majority/minority analysis. Decision trees may help to distinct problematic classes and/or misclassifications. These methods have to be applied with reasonable care since they have the potential to force the final result into one or the other direction. No standard rule exists nor can it be provided by this document. It depends on the degree of generalization how many steps of post-classification will be applied to the original classification. As a rule of thumb, we recommend to apply always a similar strategy for different scenes of the respective case study. Figure 1 demonstrates the different stages of LULC processing while figs. 2 and 3 show the LULC product for the Basel case study.

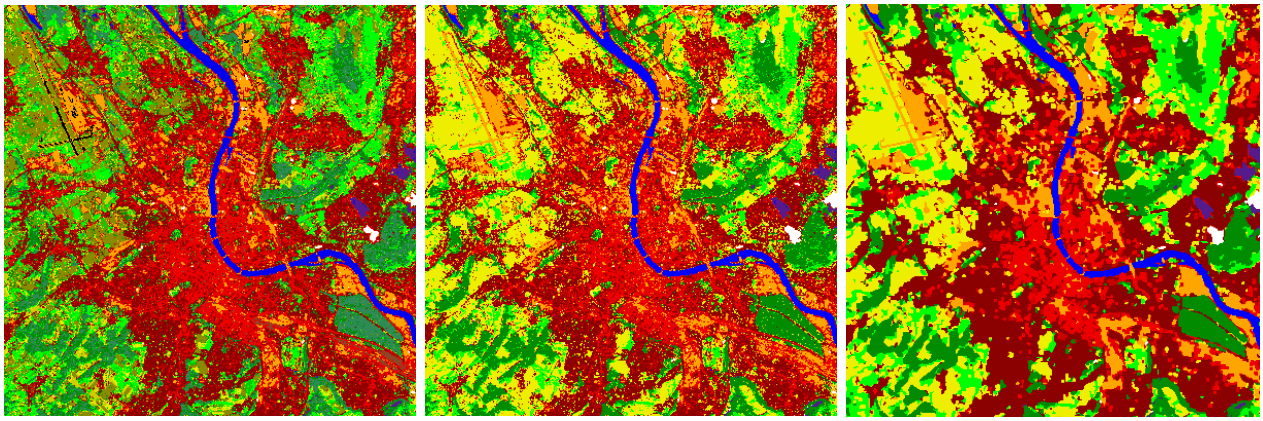

Fig. 1: Left: first MLC with several sub-classes. Center: MLC with 10 major classes according to table 2. Right: final LULC product after post-classification. Examples from Basel case study 2011.

Step 3: Quality assurance/Quality control (QA/QC): Confusion or contingency matrices are a common and well established tool for LULC accuracy analysis. This error matrix is essentially a square array of numbers organized in rows and columns which express the number of sample units (i.e. pixels and clusters of pixels) assigned to a particular category relative to the actual category as indicated by reference data (Congalton, 1996). They provide information about the accuracy of a classification by comparing the result with ground truth information. The matrix is calculated by comparing class and location of each ground truth pixel with the corresponding pixel in the classification image. The so

calculated percentage table shows the class distribution for each class. Main outputs of a confusion matrix are:

- Overall accuracy: number of correctly classified pixels divided by total number of all pixels.
- Kappa coefficient: another measure of total accuracy taking into account random errors (Stehman, 1996).
- Producer accuracy: probability that a pixel in the classification image is put into class x given the ground truth class is x
- User accuracy: probability that the ground truth class is x given a pixel is put into class x in the classification image.

Average values for MLC are about 80-85% for overall accuracy and 0.7..0.8 for the kappa-coefficient. Producer/user accuracies for the different classes vary between 60% and nearly 100%, where the residential classes show the lowest and forest and water the highest accuracies. If residential classes are combined into one single class, the accuracy is significantly increased. Note that the choice of ground truth pixels has a significant impact on the accuracy values in a confusion matrix.

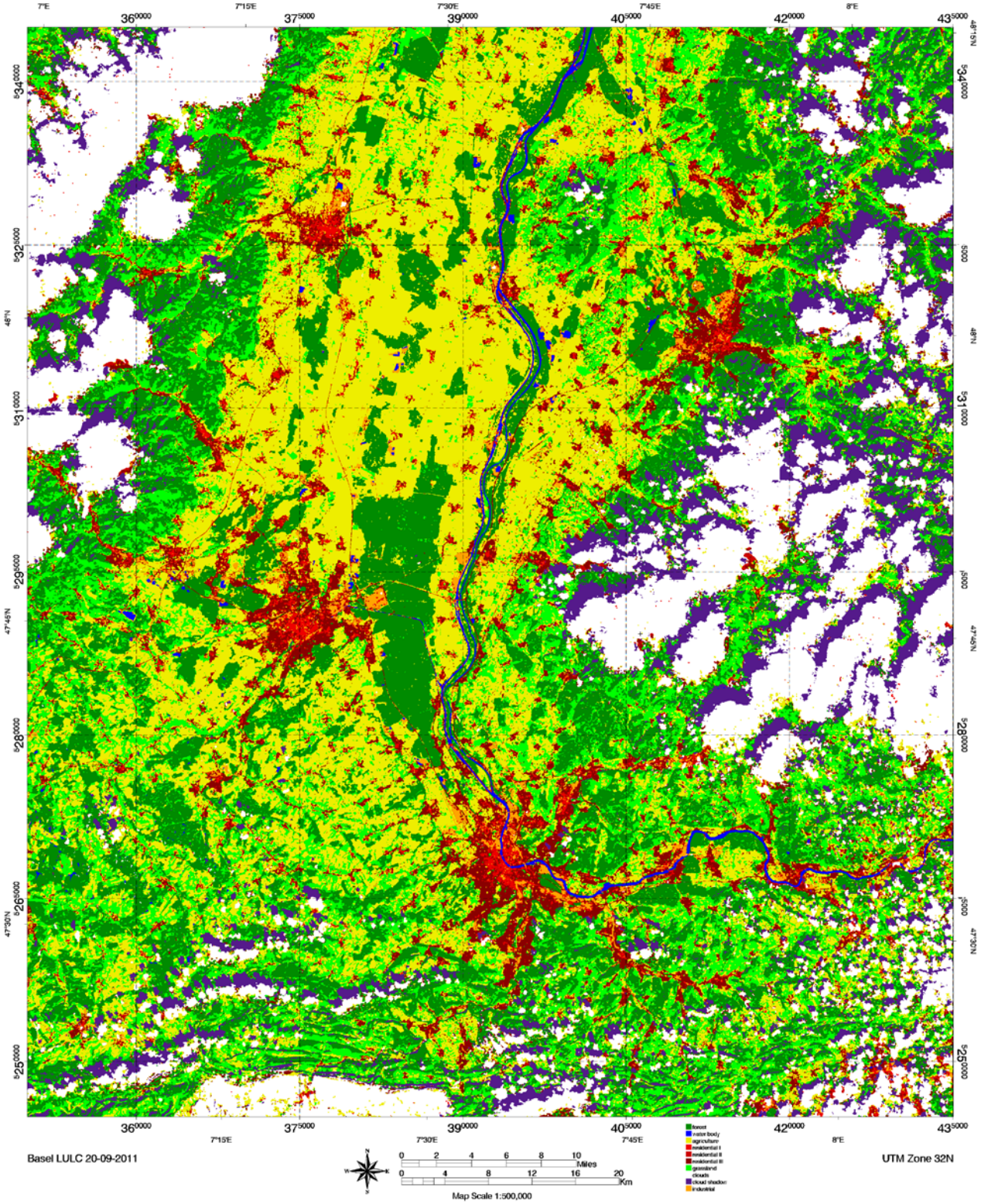

Figure 2: LULC product for the Basel region, Basel case study 2011

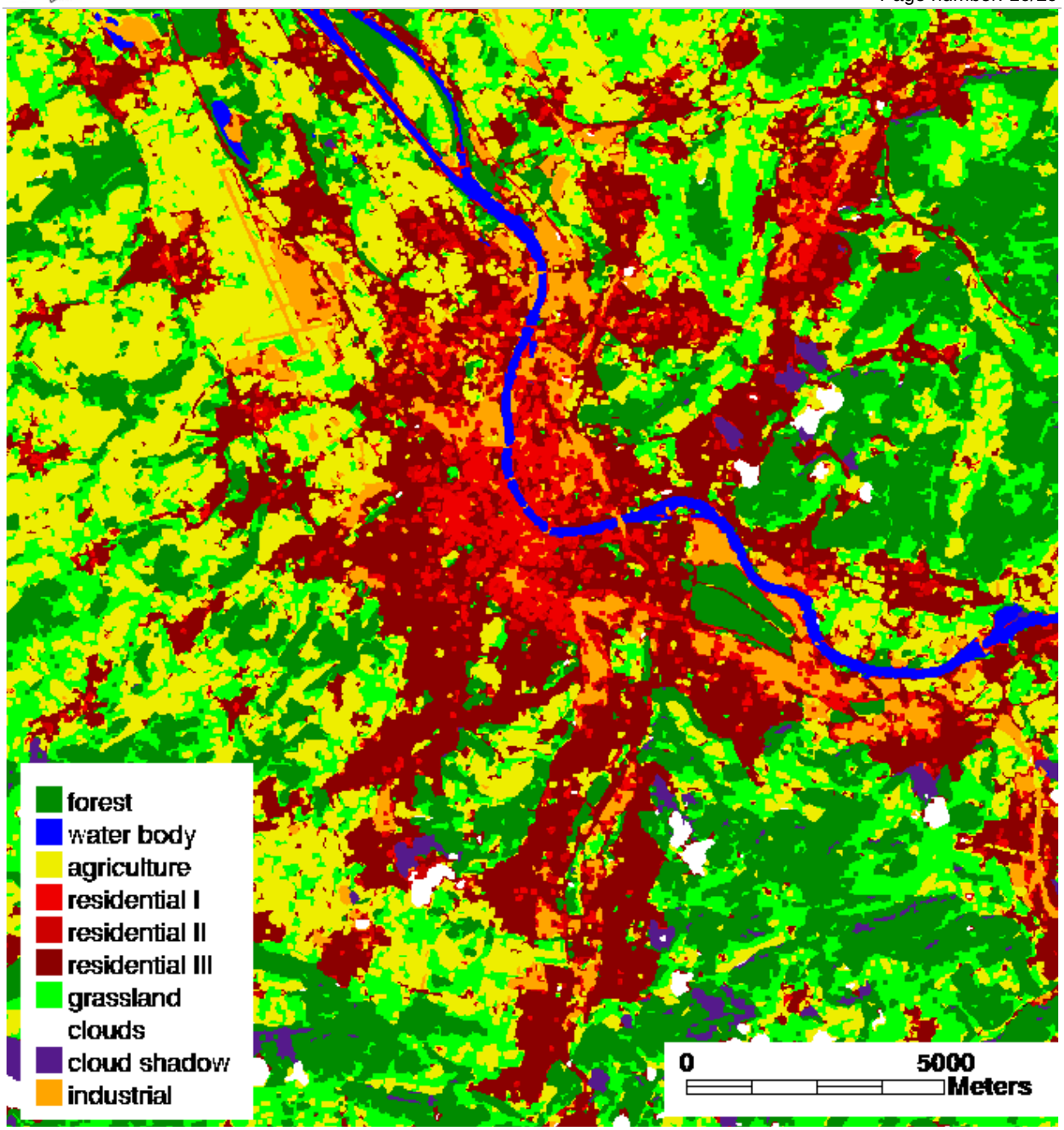

Figure 3: LULC product for the city of Basel (extraction from fig. 2), Basel case study 2011.

3.2.2 Land surface temperature (LST) and Land surface emissivity (LSE)

To retrieve Land Surface Temperature (LST) from satellite thermal infrared observations (TIR), three main effects have to be considered and corrected for: angular, emissivity and atmospheric effects. The LST retrieval accuracy varies according to both the satellite view direction, resulting in longer path-lengths through the atmosphere and thus to higher atmospheric absorption; and to the position of the sun, which angle creates a mirror effect at the anti solar point (opposite of the sun position). These directional effects, are possible source of errors that should be taken into account, especially if the spatial resolution is high, as for example in urban studies. The emissivity of land surface varies with vegetation, surface moisture, and roughness. Emissivity not only depends on the surface type but also on its physical condition imposing additional large temporal changes, make the retrieval of LST a complex undertaking, often prone to large varying and inconsistent accuracies. The three major effects of the atmosphere are absorption, upward atmospheric emission and the downward atmospheric irradiance reflected from the surface. In the 8 - 12 μm thermal infrared window region, atmospheric water vapor is mainly responsible for the atmospheric transparency, whereas the effect of the atmospheric aerosol content is smaller.

TIR channel (band 6, 10.44 μm-12.42 μm) of TM and ETM+ sensors can be used to derive brightness temperatures (black body temperatures) using Planck's law. Spectral at-sensor radiance is calculated by standard calibration:

$$L_\lambda = a * DN + b \qquad (1)$$

Scaling factors *a* and *b* are provided in the meta-information that comes with the respective Landsat scene and are also listed in Chander et al. (2009), Tables 3 and 4 for TM and ETM+, respectively.

Spectral radiance is converted to at-sensor brightness temperature (i.e. black body temperature) T_B assuming uniform emissivity by

$$T_B = \frac{K_2}{\ln\left(\frac{K_1}{L_\lambda}+1\right)}, \qquad (2)$$

where T_B is the effective at-sensor brightness temperature (K), $K_{1,2}$ are calibration constants (W m^{-2} sr^{-1} μm^{-1} and K, respectively) and L_λ is the spectral at-sensor radiance in W m^{-2} sr^{-1} μm^{-1}. Values for $K_{1,2}$ are given in the following table 3 (Chander et al., 2009).

Constant	K1	K2
units	W m^{-2} sr^{-1} μm^{-1}	K
L4 TM	671.62	1284.30
L5 TM	607.76	1260.56
L7 ETM+	666.09	1282.71

Table 3: Calibration constants for at-sensor brightness temperature

The difference between at-sensor brightness temperature T_B and land surface brightness temperature generally ranges from 1 to 5 K in the 10-12 μm region depending on atmospheric conditions (Prata et al., 1995). Atmospheric effects must therefore be considered when land surface brightness temperatures are calculated. Further on, corrections for spectral emissivity ε are needed to calculate *LST*. The error in *LST* due to the lack of knowledge of emissivity correction ranges from 0.2 to 1.2 K for mid-latitude summers (Weng et al., 2004). There are several methods for the estimation of land surface emissivity (*LSE*) derived from satellite data. The fact that TM/ETM+ only has one thermal channel inhibits the application of well-established methods based on multispectral thermal infrared images like e.g. the temperature/emissivity separation method (Gillespie et al., 1998). Alternatively, Snyder et al. (1998) proposed the derivation of *LSE* from a classification image, assigning an emissivity value to each class. Another operative and easy to apply procedure is to estimate *LSE* from the Normalized Difference Vegetation Index (*NDVI*). In the frame of GEOURBAN, of the several studies that propose this approach, we favour the application of the *NDVI* threshold method ($NDVI^{THM}$) described in Sobrino et al. (2004), because it fully covers our needs in terms of accuracy and operability. Since the main application of the *LST* product will be the analysis of urban heat island (UHI), accuracy of temperature differences is more important than absolute accuracy.

The *NDVI*^{THM} algorithm is basically a case-by-case analysis of the *NDVI*. The calculation of the *NDVI* is described in section 3.2.4. The different cases are:

- NDVI < 0.2: pixel considered as bare soil, ε = 0.97 (derived from soil spectra in the ASTER spectral library filtered according to TM/ETM+ band 6 filter function)
- NDVI > 0.5: pixel considered as fully vegetated ε = 0.99
- 0.2 ≤ NDVI ≤ 0.5: pixel considered as a mixture of bare soil and vegetation, ε is calculated as follows:

$$\varepsilon = 0.004 * \mathrm{P_V} + 0.986, \qquad (3)$$

where P_V is the vegetation fraction of the pixel according to Carlson and Ripley (1997):

$$\mathrm{P_V} = \left[\frac{\mathrm{NDVI} - \mathrm{NDVI_{min}}}{\mathrm{NDVI_{max}} - \mathrm{NDVI_{min}}}\right]^2, \qquad (4)$$

with $NDVI_{min,max}$ as 0.2 and 0.5, respectively. Following the argumentation in Sobrino et al. (2004), several assumptions regarding the effects of geometrical distribution, internal reflections and the roughness of surfaces, emissivity values for vegetation and, more critical, soil have been made to arrive at the final expression in eq. (4).

An emissivity corrected *LST* can then be calculated after Artis & Callahan (1982) by:

$$\mathrm{LST} = \frac{\mathrm{T_B}}{1 + \left(\lambda * \frac{\mathrm{T_B}}{\rho}\right) \ln\varepsilon}, \qquad (5)$$

where T_B is at-sensor brightness temperature from eq. (1), λ effective wavelength of TM/ETM+ band 6 ($11.57 * 10^{-6}$ m), $\rho = c * h / \sigma$ ($1.438 * 10^{-2}$ m K), σ = Boltzmann constant ($1.38 * 10^{-23}$ J/K), h = Planck's constant (6.626 *10-34 J s) and c = velocity of light ($2.998 * 10^8$ m/s). Figure 4 shows the function in eq. (5) for emissivities in the range of 0.95..0.99, Figure 5 shows the final LST product for the Basel case study.

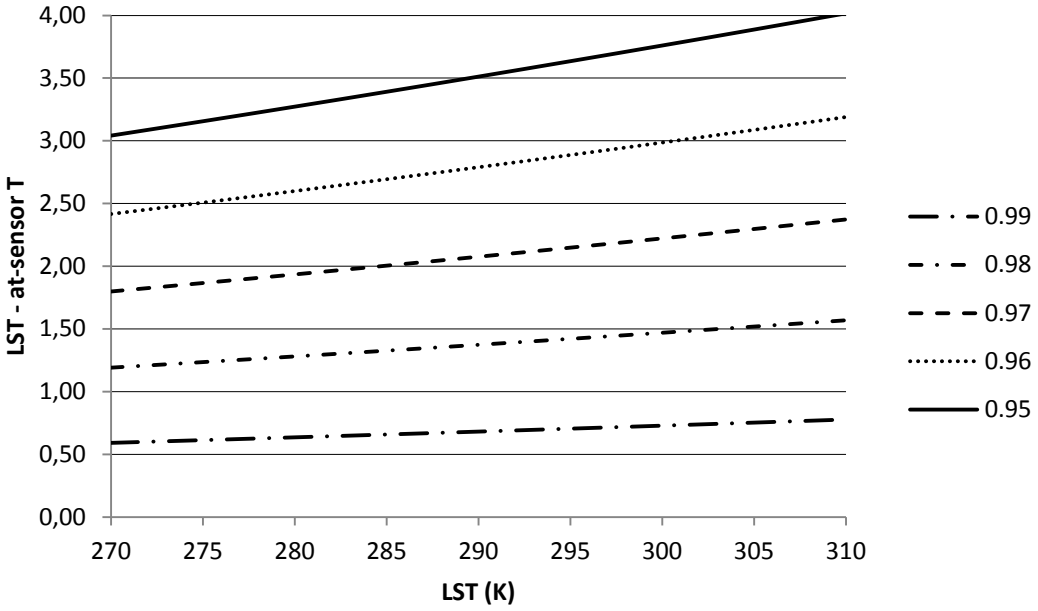

Fig. 4: Difference between *LST* and at-sensor temperature T_B for emissivity ranging from 0.95 to 0.99.

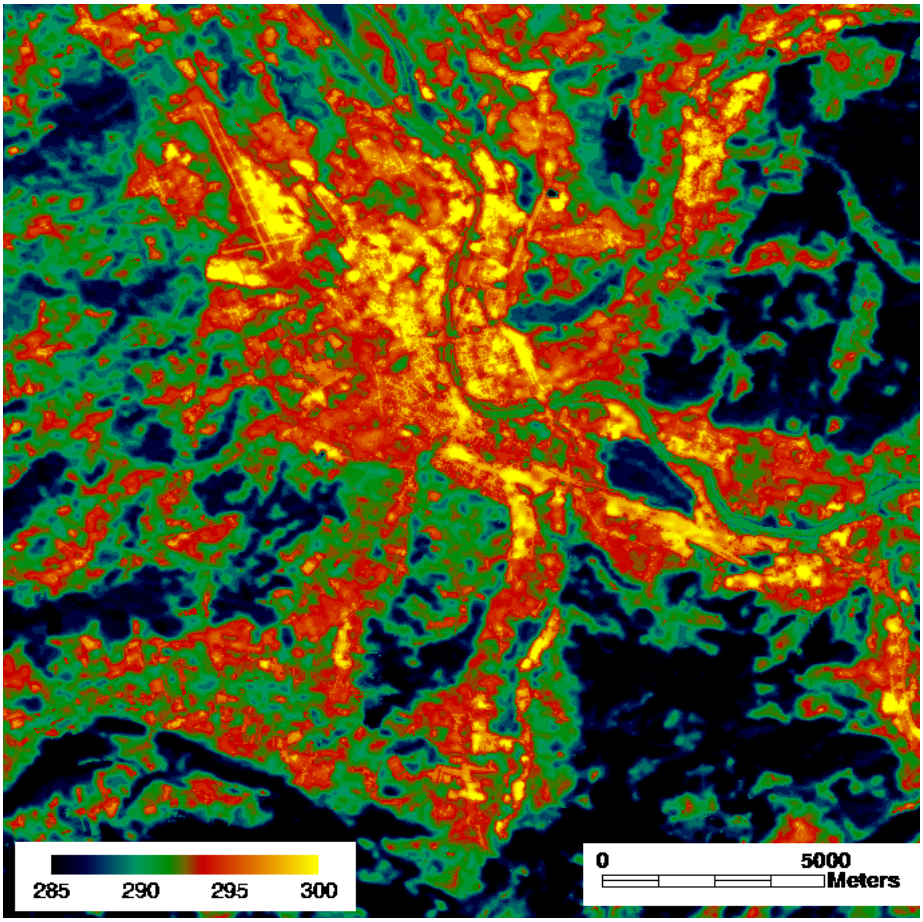

Fig. 5: LST product derived from Landsat TM, Basel case study 2011.

3.2.3 Broadband albedo

The urban land surface broadband albedo is an important variable in the radiation balance and has significant impacts on the urban energy balance. The “Cool Roofs Project” in the frame of the R20 Regions of climate action (www.regions20.org) and the propagation of “Cool Roofs” and “Cool Pavements” technologies by the U.S. Environmental Protection Agency (www.epa.gov) are illustrious examples on how the effect of shortwave broadband albedo is included in urban planning and urban heat island mitigation strategies, amongst many others. Top-of-atmosphere (TOA) multispectral sensors like Landsat TM/ETM+ monitor effectively the atmospheric conditions and surface characteristics which can be used for the derivation of land surface broadband albedo. Among several types of broadband albedos the total shortwave albedo covering the wavelength range from about 0.4…2.5 μm is of main interest for urban planning purposes. The derivation of surface broadband albedos from narrow-band observations requires three main steps of processing, namely a) atmospheric correction that converts at-sensor radiance to surface directional reflectance, b) application of BRDF functions that convert directional reflectance to spectral albedo, and c) spectral to broadband albedo conversion. If the surface is assumed to be Lambertian, step b) may be omitted. Further on, the derivation of angular functions for three dimensional surfaces (the usual case in urban environments) is a difficult task and out of the scope of this project. The MODIS BRDF/albedo product may serve as a more accurate alternative for regional applications; however, its resolution of 500 m does not meet the scale requirements for urban planning.

For the GEOURBAN albedo product we applied the conversion algorithm for Landsat TM/ETM+ surface spectral reflectance as published by Liang (2000). This study provides narrowband to broadband albedo conversion formulae for a series of multispectral sensors derived from extensive radiative transfer simulations under different surface and atmospheric conditions. The results of these conversion formulae have been validated in Liang et al. (2002) and have been shown to be very accurate. The wavelength range from 0.4…2.5 μm also corresponds to the albedo that is usually reported from ground measurements using pyranometers. Such measurements are widely available and therefore the validation of the conversion formulae can be performed with a large number data for a large variety of surface types. The accuracy of the reported average residual

standard error (RSE) of 0.02 for the TM/ETM+ conversion formula (assuming Lambertian surface) fulfills the needs of an albedo product for urban planning purposes. Figure 6 shows the albedo product for the Basel case study.

Narrowband to broadband conversion formula for Landsat TM/ETM+ after Liang (2000):

$$\alpha = 0.356\alpha_1 + 0.130\alpha_3 + 0.373\alpha_4 + 0.085\alpha_5 + 0.072\alpha_7 + 0.0018 \qquad (6)$$

with: α total shortwave albedo

α_x spectral surface reflectance of TM/ETM+ band x

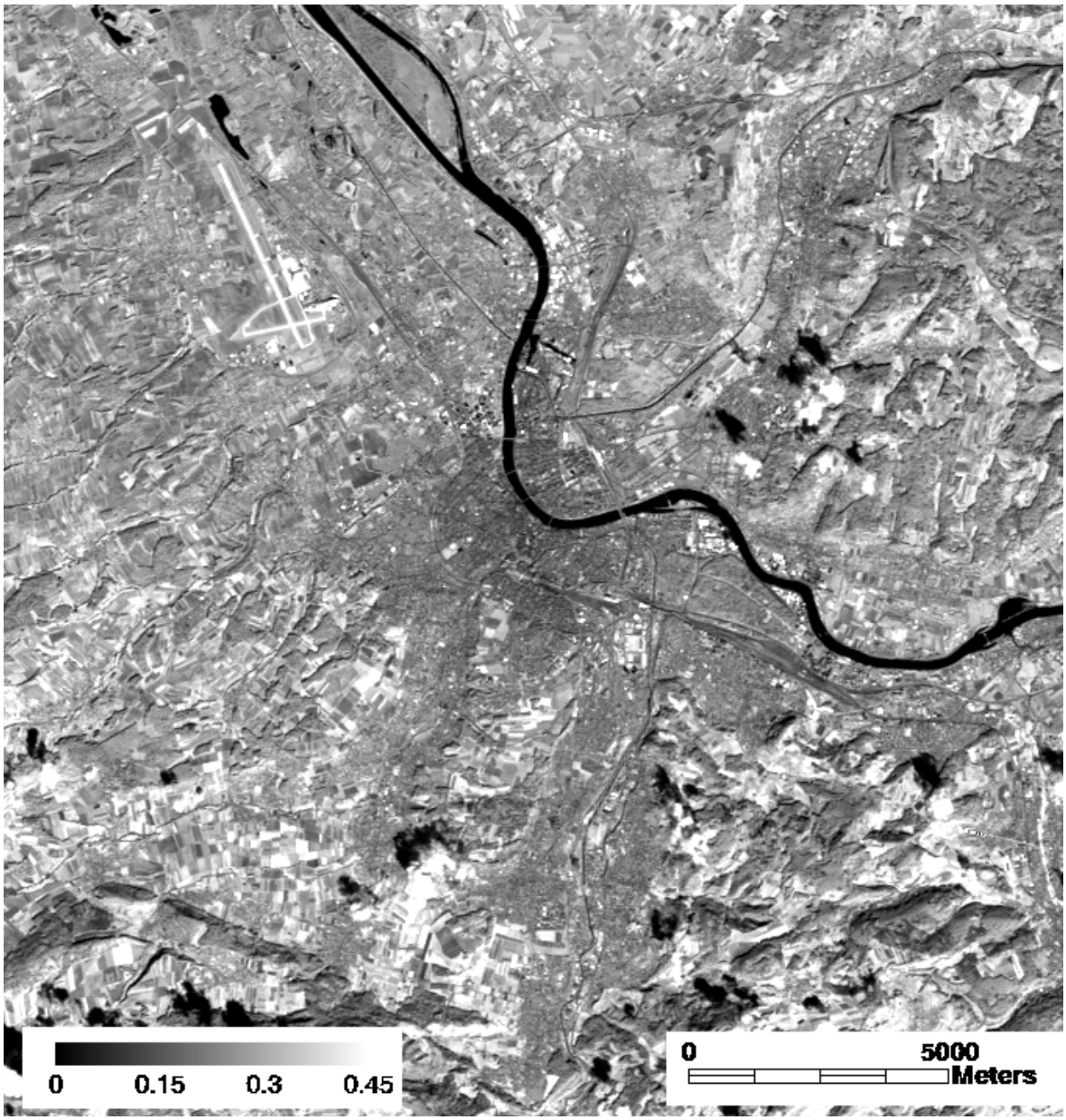

Fig. 6: Broadband albedo, Basel case study 2011

3.2.4 Normalized Difference Vegetation Index (NDVI)

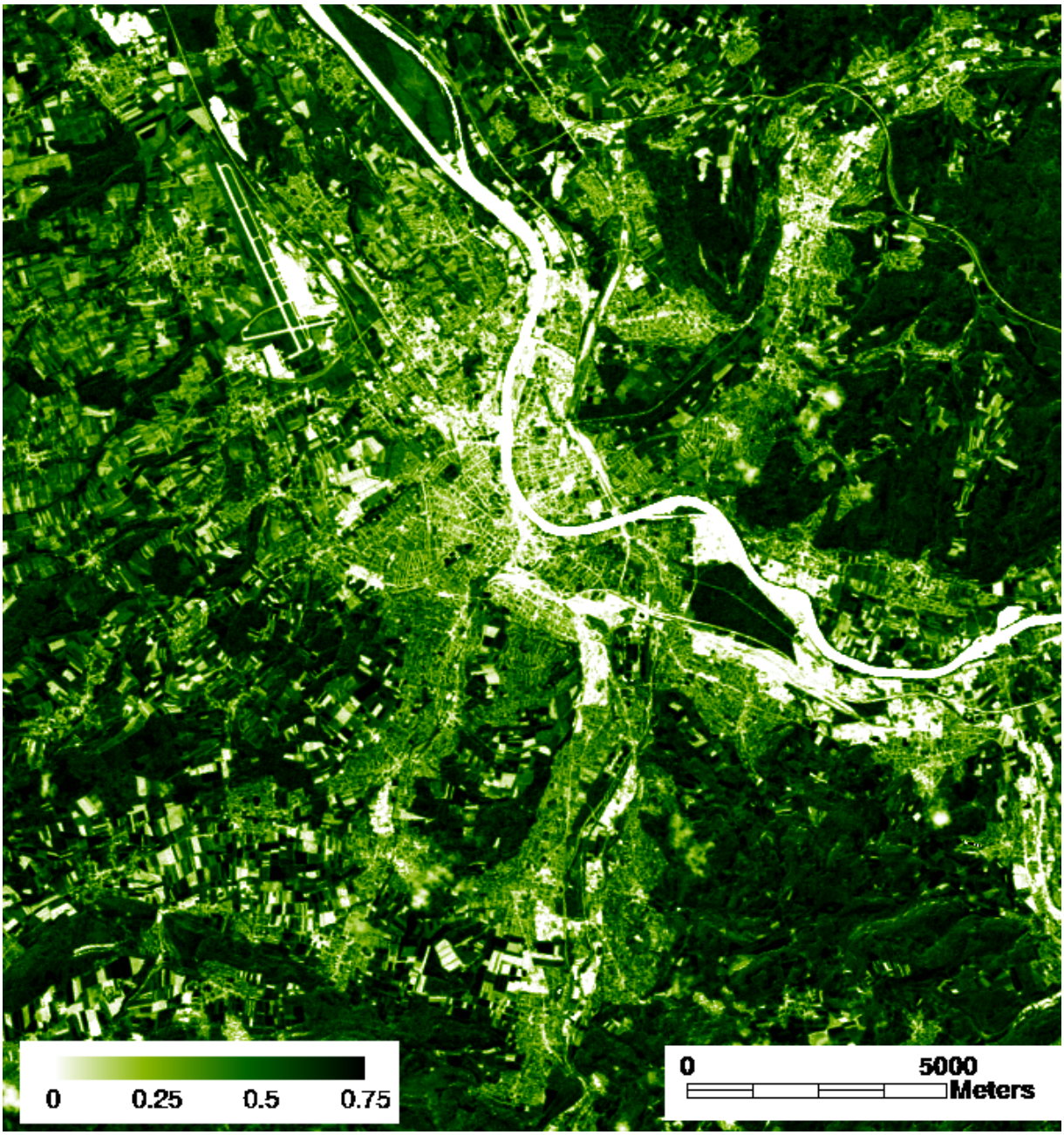

Fig. 7: NDVI, Basel case study 2011

NDVI values are, amongst other, necessary for the retrieval of *LSE* as described in section 3.2.2. *NDVI* is a well-established index and widely used in numerous applications in the remote sensing community. It is basically calculated from red and near infrared bands, in the case of Landsat this conforms to TM/ETM+ bands 3 and 4, respectively.

$$\mathrm{NDVI} = \frac{\mathrm{TM4}-\mathrm{TM3}}{\mathrm{TM4}+\mathrm{TM3}}, \qquad (7)$$

Although *NDVI* calculation is a standard procedure and implied in most common imaging software, it has to be kept in mind that *NDVI* calculated from at-sensor reflectance can be considered as a first approximation, but it is more accurate to use surface reflectance values as input data for eq. (7). For preprocessing of Landsat data refer to section 3.1. The NDVI product for the Basel case study is shown in Fig. 7.

3.3 MODIS

The Moderate Resolution Imaging Spectroradiometer (MODIS) is a sensor on board the NASA Earth Observing System Terra and Aqua satellites. Terra was launched on 18 December 1999 and Aqua on 4 May 2002. Both satellites are polar orbiting, covering the entire Earth's surface every 1 to 2 days, and crossing the equator at approximately 10:30 (Terra) and 13:30 (Aqua) local time. MODIS acquires data in 36 spectral bands, ranging from the visible through the near-IR and mid-IR to the thermal IR (0.405 – 14.385 μm). MODIS data are being used operationally to provide a variety of geophysical parameters employed in monitoring the Earth's land, ocean and atmosphere in several temporal and spatial resolutions. MODIS data is freely available from the NASA Level 1 and Atmosphere Archive and Distribution System (LAADS Web) on http://ladsweb.nascom.nasa.gov/data/. Using this interface, the user can select between Terra and Aqua satellites, different collections, products and processing levels (Levels 1, 2 and 3) of MODIS data.

Three products from the MODIS palette are considered for use in GEOURBAN, namely the MODIS Land Cover Type product (MCD12), MODIS Land Surface Temperature and Emissivity (MOD11A1) and the MODIS AOT which is included in the MODIS level 2 Aerosol product (MOD04_L2). However, the low resolution of these products (500 m for LULC, 1000 m for LST, 10 km for AOT) considerably limits its practical use for urban planning purposes. The MODIS products therefore mainly serve as an additional supporting source of information and, in the case of LULC, albedo and LST, as a rough validation for similar Landsat derived products. Because the MODIS products are used in GEOURBAN as provided by NASA and no additional processing is applied, we refer to the to the relevant MODIS websites (http://modis.gsfc.nasa.gov/index.php and http://ladsweb.nascom.nasa.gov) for additional information for the respective product.

MODIS products are included in the HDF-file of the Scientific Data Sets (SDS) and can be exported, (de)scaled, resampled and reprojected with most standard EO and data processing software packages. A selection of tools for MODIS data for several software packages (including the MODIS conversion toolkit for ENVI) is available from http://nsidc.org/data/modis/tools.html and/or http://modis-land.gsfc.nasa.gov/tools.html. MODIS products AOT, LST and LULC for the three GEOURBAN case studies are also available from the GEOURBAN ftp-server.

3.4 MODIS products

3.4.1 MODIS Land surface temperature (LST day/night)

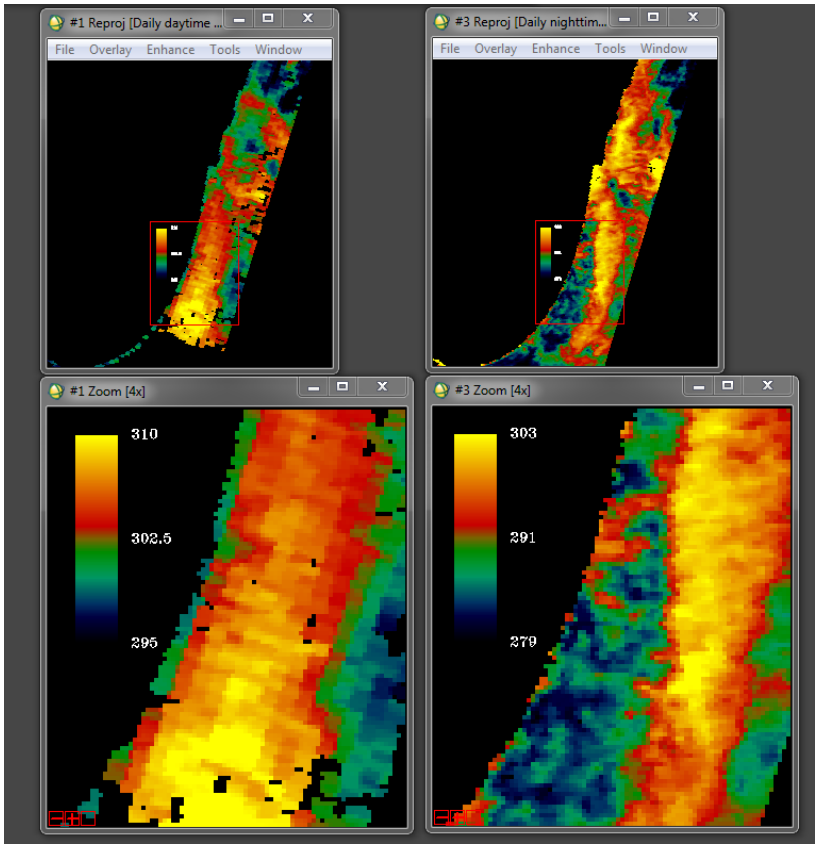

Fig. 8: MODIS LST product for day (left) and night (right). Data from DOY 337 2010. Resolution 1000 m. Tel Aviv case study.

The daily level 3 LST product at 1 km spatial resolution is a tile of daily LST product gridded in the Integerized Sinusoidal projection (in V3) or the Sinusoidal projection (in V4). A tile contains 1200 by 1200 grids in 1200 rows and 1200 columns. The exact grid size at 1km spatial resolution is 0.928km by 0.928km. The Scientific Data Set (SDS) of the MOD11A1 includes a daily daytime/nighttime 1km grid of Land-surface Temperature, amongst other. For a comprehensive description of the MODIS LST product refer to the MODIS Land Surface Temperature Products Users' Guide (Wan, 2005).

3.4.2 MODIS Land use/Land cover (LULC)

The MODIS Terra+Aqua Combined Land Cover product incorporates five different land cover classification schemes, derived through a supervised decision-tree classification method. The primary land cover scheme identifies 17 classes defined by the IGBP, including 11 natural vegetation classes, three human-altered classes, and three non-vegetated classes. Detailed information about the MODIS Land Cover Type products is available on the MODIS Land Website (http://modis-land.gsfc.nasa.gov/index.html). Figure 9 shows an example for the Tel Aviv case study.

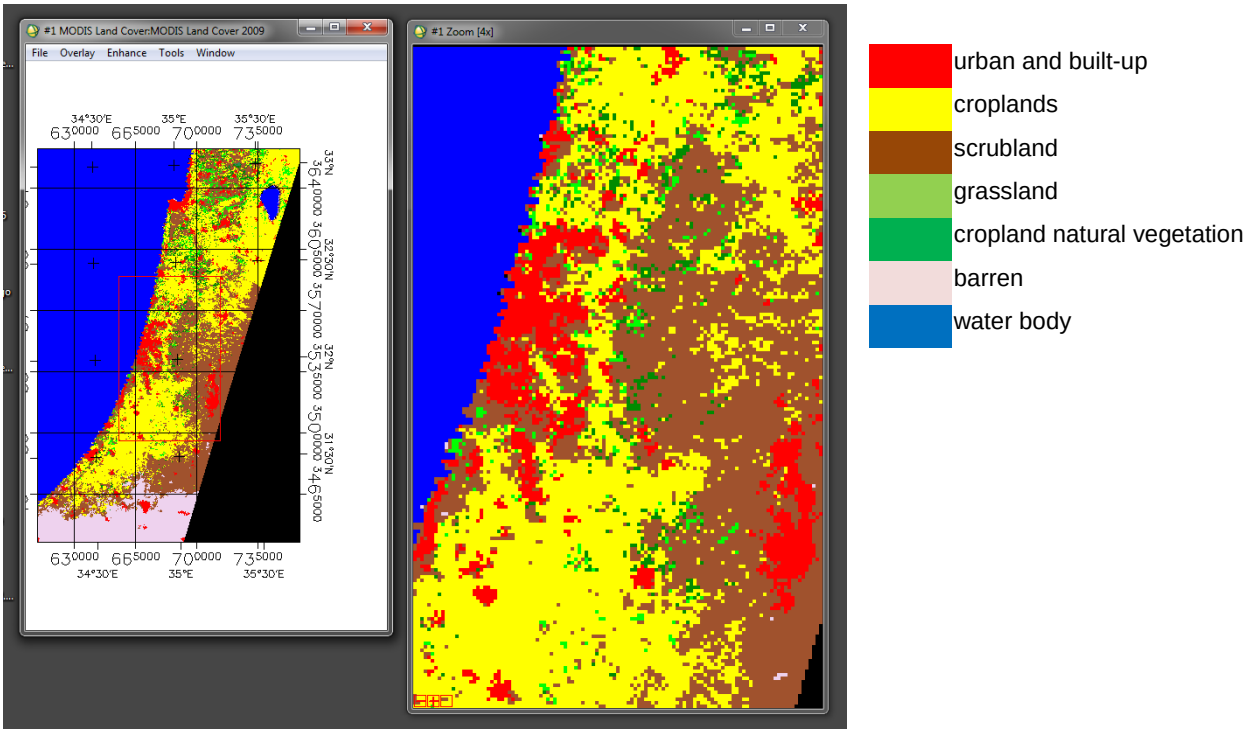

Fig. 9: MODIS Land Cover 2009, type I (IGBP classification scheme). Resolution 500 m. Tel Aviv case study (UTM coordinates).

3.4.3 MODIS Aerosol Optical Thickness (AOT)

Regarding the atmosphere, Level 2 data are grouped in several products, which include: the Aerosol Product, which monitors aerosol properties, the Cloud Product, monitoring cloud physical and optical parameters, the Atmosphere Profile Product, which includes profiles of atmospheric temperature and moisture, atmospheric stability and total ozone, and the Water Vapor product, monitoring atmospheric water vapor and precipitable water. A detailed description of the MODIS Aerosol product can be found in Remer et al. (2005).

The most updated and validated MODIS Level 2 Collection (C051) comprises of Hierarchical Data Format (HDF) files of all Products, spanning the entire Terra and Aqua operational periods (February 2000 and July 2002 until present, respectively). Each HDF file contains datasets of various parameters, corresponding to 5 minutes of data acquisition. In the case of the Aerosol Product, the spatial resolution ranges between ~10 km × 10 km at nadir and ~20 km × 20 km at the edge of the swath. The MODIS daily AOT at 10 km × 10 km spatial resolution is included in the Level 2 Aerosol Product of the Atmosphere Level 2 Products Group. Temporal selection (starting and ending date and time) and spatial selection (definition of an area of interest using geographical coordinates) are also included. The Collection Selection drop-down list allows the user to select among different Collections, each one representing a different processing algorithm used. While Collection 6 is the latest available, Collection 5.1 is the latest Collection which has been thoroughly validated, as far as aerosol parameters are concerned. The Metadata Selection allows the user to apply quality and successful retrieval filters to the search results. In Fig. 10 the AOT values are given for the Basel area, where the administrative political boundaries are also displayed.

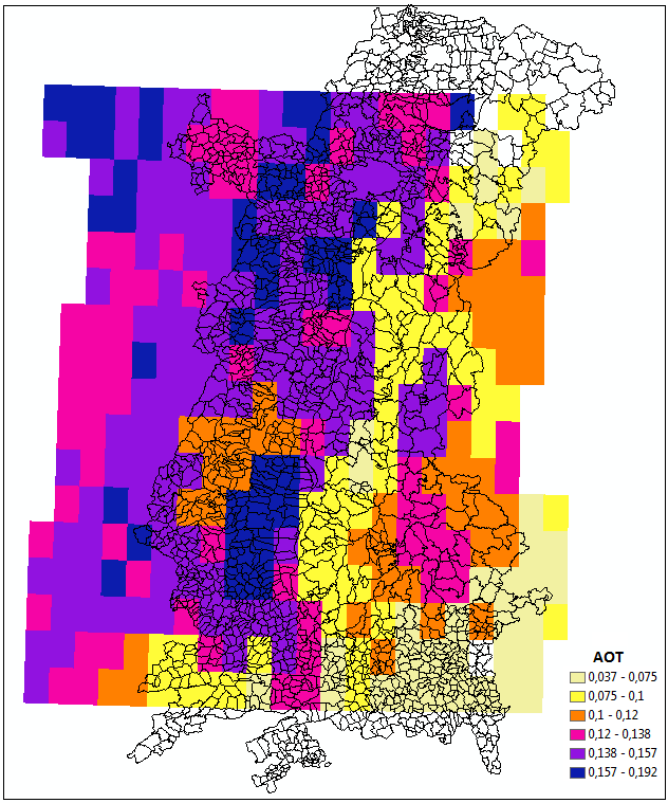

Fig. 10: AOT map produced by MODIS (2012 image) for Basel Area

3.5 Digital Terrain Model (DTM): SRTM

The Shuttle Radar Topography Mission (SRTM) from February 2000 generated the most complete HR- digital topographic database of Earth. The Digital Terrain Model for case studies Basel, Tel Aviv and Tyumen are used in GEOURBAN as provided by NASA's Jet Propulsion Laboratory (JPL) with no further processing. Fig. 11 shows an example of the DTM product for the Tyumen region. For further information about SRTM we refer to Farr et al. (2007) and the JPL SRTM website (http://www2.jpl.nasa.gov/srtm/).

SRTM data are available from http://dds.cr.usgs.gov/srtm/ and from the GEOURBAN ftp-server for GEOURBAN case studies.

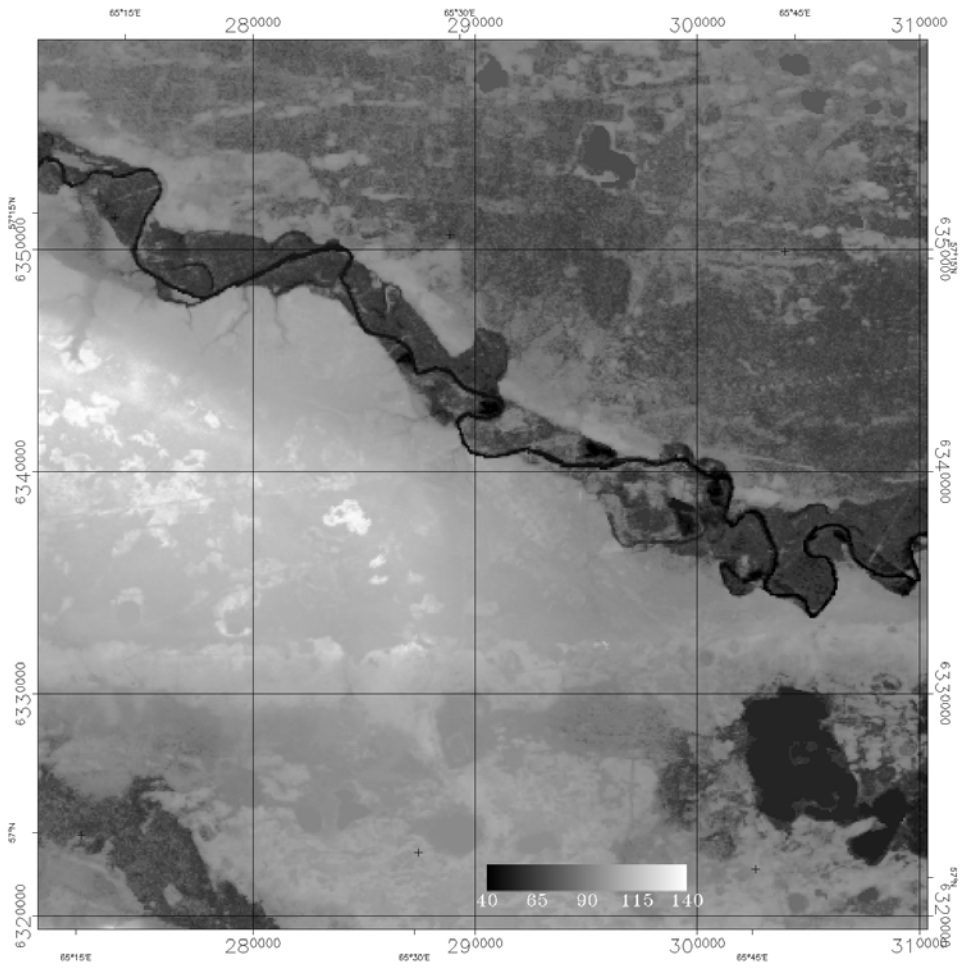

Fig. 11: SRTM Digital Terrain Model (DTM) for Tyumen region (UTM coordinates).

3.6 The ASTER Global DEM (GDEM)

The most recent global DEM source is the ASTER Global Digital Elevation Model (GDEM) which was released by Japan's Ministry of Economy, Trade and Industry (METI) and United States National Aeronautics and Space Administration (NASA) on June 29, 2009. GDEM is a global DEM generated using ASTER data, with 30 m posting. The ASTER GDEM was created by stereo-correlating the entire ASTER archive; stacking and averaging the individual DEMs; cloud screening; filling voids or holes using SRTM 3 arc-second data; and validating the GDEM against higher resolution DEMs worldwide. Despite its high spatial resolution (30m posting) GDEM was found to contain significant anomalies, which will affect its usefulness for certain user applications. Given that the water bodies can be effectively masked in ASTER imagery, there are two primary sources of these anomalies. One is residual clouds in the ASTER scenes used to generate the GDEM, and the other is the algorithm used to generate the final GDEM from individual ASTER DEMs available to contribute to the final elevation value for any given pixel.

A detailed study compared conterminous United States (CONUS) GDEM data (934 GDEM tiles) to the United States Geological Survey (USGS) National Elevation Dataset (NED) and calculated an overall vertical Root Mean Square Error (RMSE) of 10.87 m (GDEM Validation Team 2009). When compared with more than 13,000 GCPs from CONUS, the RMSE dropped to 9.37 meters (Abrams et al. 2010). GDEM has been also validated for the whole area of Greece by Chrysoulakis et al (2011). They found a vertical accuracy of around 20 m (RMSE = 11.08 m) when GDEM derived elevations were compared with GPS derived elevations.

ASTER GDEM Version 2 was released on October 17, 2011. This data for any specific location can be downloaded from: http://www.jspacesystems.or.jp/ersdac/GDEM/E/ 4.html